

Nonseparable Gaussian Stochastic Process: A Unified View and Computational Strategy

Mengyang Gu and Yanxun Xu

Department of Applied Mathematics and Statistics, Johns Hopkins University, Baltimore, MD

Abstract

Gaussian stochastic process (GaSP) has been widely used as a prior over functions due to its flexibility and tractability in modeling. However, the computational cost in evaluating the likelihood is $O(n^3)$, where n is the number of observed points in the process, as it requires to invert the covariance matrix. This bottleneck prevents GaSP being widely used in large-scale data. We propose a general class of nonseparable GaSP models for multiple functional observations with a fast and exact algorithm, in which the computation is linear ($O(n)$) and exact, requiring no approximation to compute the likelihood. We show that the commonly used linear regression and separable models are special cases of the proposed nonseparable GaSP model. Through the study of an epigenetic application, the proposed nonseparable GaSP model can accurately predict the genome-wide DNA methylation levels and compares favorably to alternative methods, such as linear regression, random forests and localized Kriging method.

KEY WORDS: Exact computation, Fast algorithm, Methylation levels imputation, Multiple functional data, Stochastic differential equations

1 Introduction

The increasing demands to analyze high dimensional data with complex structures have facilitated the development of novel statistical models for functional data, in which the outcomes can be interpreted as samples of random functions. Time series, longitudinal, and spatial data are some typical examples of functional data. One common feature among functional data is that, often, the linear regression does not appropriately explain the correlations between the outcomes that are close in the inputs of the function. The correlation is often expressed through a mapping from the functional inputs to the associated outcomes, usually modeled as a stochastic process, and the correlations between nearby inputs are captured through a covariance matrix. One natural choice of such stochastic process is the Gaussian stochastic process (GaSP), which has been widely used in many applications (Sacks et al., 1989; Bayarri et al., 2009; Gelfand et al., 2010).

GaSP models have also been popular in analyzing functional data with multiple functional outcomes, in which independent GaSP models are generally built separately for each outcome for simplicity. A more sophisticated approach is to define a separable GaSP model, where the correlations between functions and between inputs are modeled separately using a matrix normal distribution (Conti and O’Hagan, 2010). Other approaches include estimating a basis function, such as using the principal component analysis (Higdon et al., 2008), with the weights of the basis functions modeled as independent GaSPs to model the correlation structure over the input space. This construction results in *nonseparable* covariance structures, meaning that the covariance matrix cannot be decomposed as a Kronecker product of two small covariance matrices.

For large-scale data, a GaSP model is often computationally expensive: the evaluation of the likelihood requires $O(n^3)$ computational operations to compute the inverse of the covariance matrix, where n is the number of observed data points. To ease the computa-

tion, many approximation methods have been proposed, including low rank approximation (Banerjee et al., 2008), covariance tapering (Kaufman et al., 2008), use of Gaussian Markov random field representations (Lindgren et al., 2011), and likelihood approximation (Eidsvik et al., 2013). Those approximation methods are sometimes preferred for computationally intensive problems, however, the exact computation is more desired if we can overcome the $O(n^3)$ computational operations.

Our motivating study is to impute millions of DNA methylation levels at CpG sites across the human genome. DNA methylation is an epigenetic modification of DNA, playing important roles in DNA replication, gene transcription, aging, and cancer evolution (Das and Singal, 2004; Scarano et al., 2005). Methylation levels are quantified at every genomic CpG site, a region of DNA where a cytosine (C) nucleotide is followed by a guanine (G) nucleotide in the linear sequence of bases along its 5' to 3' direction. Single-site DNA methylation level can be quantified by whole-genome bisulfite sequencing (WGBS), in which approximately 26 million CpG sites in the human genome are evaluated for whether they are methylated or not. However, WGBS is expensive and hard to examine in certain genomic regions. This motivates alternative methylation assay technologies, such as Illumina HumanMethylation450 BeadChip (henceforth, Methylation450K) that measures DNA methylation levels at approximately 482,000 CpG sites (less than 2% of the total number of CpG sites). The goal is to impute DNA methylation levels at the CpG sites that are observed in the WGBS samples but unobserved in the Methylation450K data by exploiting the correlations among the full set of CpG sites in the WGBS samples.

The empirical correlation of methylation levels with distance smaller than 5000 bases in the WGBS samples is shown in the left panel of Figure 1. For each integer distance, we calculate the empirical correlation of every possible pair with this distance. The blue dots in the left panel are the average correlation of the methylation levels between two CpG sites at a given CpG distance smaller than 5000 bases. The methylation levels at nearby CpG sites

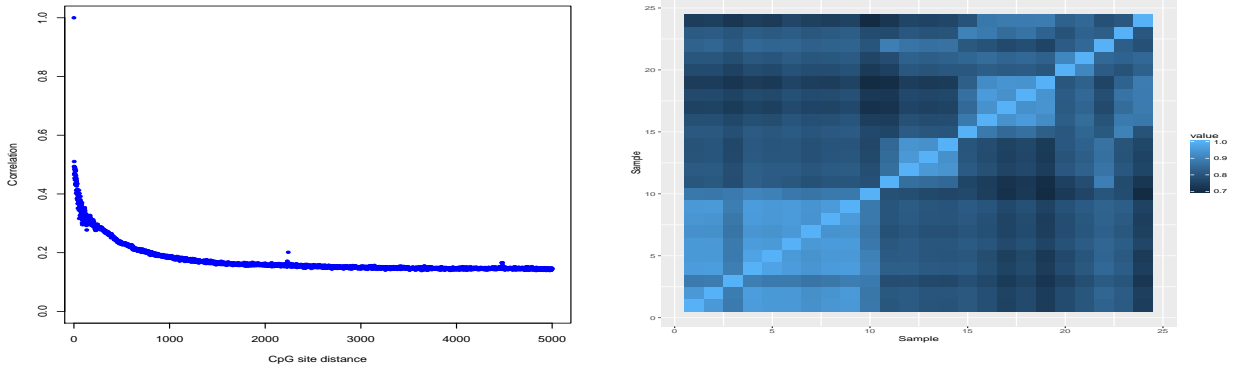


Figure 1: Empirical correlation of methylation levels across sites (left panel) and across samples (right panel). The number of samples is 24 and each sample has 1.6 million methylation levels.

are correlated to each other on average and the correlation gradually decays as the distance between the two CpG sites increases. Such phenomenon is called co-methylation and has been observed in previous studies (Zhang et al., 2015). Furthermore, as shown in the right panel of Figure 1, methylation levels for each CpG site across samples are well correlated for biological reasons. Since methylation plays important roles in suppressing gene expression levels, they are tightly regulated in cells and variability of such regulations is associated with disease risk (Das and Singal, 2004). Understanding the correlation patterns in methylations levels is thus meaningful for reducing the risk of diseases. These empirical findings motivate us to develop a statistical model to exploit the correlations of methylation levels across the unequally-spaced genome sites and across different samples for the goal of imputation.

In this paper, we develop a computationally efficient model to impute the methylation levels. Our contribution is three-fold. First, we propose a nonseparable GaSP model to integrate different correlation structures among the methylation levels across genome sites and across samples into a coherent model, while the previous regression method (Zhang et al., 2015) ignores the correlations across samples. Second, we develop an ultra-fast algorithm that computes the exact likelihood of the proposed nonseparable GaSP model with $O(n)$ computational operations and storage when using a large class of covariance functions,

building upon the connection between the Gaussian random field and Gaussian Markov random field (Hartikainen and Sarkka, 2010). Lastly, the proposed nonseparable GaSP model can be seen as a general statistical framework that unifies the linear regression and separable GaSP models. Though we focus on methylation levels imputation in this work, the methodology is widely applicable to many other studies, such as estimating the response curve from the electronic health record data, where each patient’s visit is modeled as a function of time (Xu et al. (2016)).

The rest of the paper is organized as follows. In Section 2, we study a class of nonseparable GaSP models. The closed form marginal likelihood and predictive distribution are derived for the imputation problem. In Section 3, the computational strategy for this class of nonseparable GaSP models is introduced, for which the computation scales linearly in the number of inputs of the function without approximation. In Section 4, we unify some other frequently used approaches, such as the linear regression and separable GaSP models, under the framework of the nonseparable GaSP models. Numerical examples and comparisons to alternative methods are provided in Section 5. We conclude the paper with discussion and future extensions in Section 6.

2 Modeling multiple functional data

Let $y_i(s_j)$ be the methylation level of the i^{th} sample at the j^{th} CpG site, recording the proportion of probes for a single CpG site that is methylated, for $i = 1, \dots, K$, $j = 1, \dots, N$. Define two groups of sites, $\mathbf{s}^{\mathcal{D}} = \{s_1^{\mathcal{D}}, \dots, s_n^{\mathcal{D}}\}$ and $\mathbf{s}^* = \{s_1^*, \dots, s_{n^*}^*\}$, where the methylation levels of $\mathbf{s}^{\mathcal{D}}$ are observed for all K samples and the methylation levels of $\mathbf{s}^* = \{s_1^*, \dots, s_{n^*}^*\}$ are only available for the first k samples but not available for the last k^* samples. The total number of samples is $K = k + k^*$ and the total number of CpG sites is $N = n + n^*$.

For the first k samples, methylation levels are measured at all CpG sites, meaning that

we observe $\mathbf{y}(\mathbf{s}^{\mathcal{D}})_{[k \times n]}$ and $\mathbf{y}(\mathbf{s}^*)_{[k \times n^*]}$. However, for the remaining k^* samples, the methylation levels are only observed at a small subset of CpG sites, denoted as $\mathbf{y}^*(\mathbf{s}^{\mathcal{D}})_{[k^* \times n]}$. The methylation levels at the remaining CpG sites ($\mathbf{y}^*(\mathbf{s}^*)_{[k^* \times n^*]}$) of these samples are unknown. Our goal, then, is to interpolate the unobserved methylation levels of these k^* samples using their observed methylation values at n CpG sites and the full methylation values from the other k samples. In other words, we seek the predictive distribution of $\mathbf{y}^*(\mathbf{s}^*)$ conditional on $\mathbf{y}(\mathbf{s}^{\mathcal{D}})$, $\mathbf{y}(\mathbf{s}^*)$ and $\mathbf{y}^*(\mathbf{s}^{\mathcal{D}})$.

The imputation of methylation levels across the whole genome is computationally challenging due to the large number of CpG sites. In the full WGBS data set, there are about 2.8×10^7 CpG sites; even in the smaller Methylation450K data, there are roughly 4.5×10^5 CpG sites, creating computational challenges. In contrast, the number of samples we are working with is relatively small: 24 samples in the WGBS data and 100 samples in the Methylation450K data. The key advantage of our method is that the computation required for imputation scales linearly in terms of the number of CpG sites.

Here we make several extensions of a class of GaSP models with the nonseparable structure, which has been used for modeling multivariate spatially correlated data and functional outputs (Gelfand et al., 2004; Higdon et al., 2008). First of all, we construct a flexible way to incorporate the correlations across samples and across sites for prediction, with closed form expression of the marginal likelihood and predictive distribution. These expressions enable us to establish the connection between this nonseparable model and other models, such as the linear regression and separable models, discussed in Section 4. Furthermore, we introduce a computationally feasible approach to large-scale problems with inputs (CpG sites) up to a million without approximating the likelihood function. The proof of this section is given in Appendix A. Without loss of generality, we assume the data are centered at zero. An extension to combine site-specified features is given in the supplementary materials.

2.1 Nonseparable GaSP model with homogeneous noises

We start with the model for the functional output, $Y(s)$, for every site $s \in \mathcal{S}$

$$\mathbf{Y}(s) = \mathbf{A}\mathbf{v}(s) + \boldsymbol{\epsilon}_0, \quad (1)$$

where $\boldsymbol{\epsilon}_0 \sim N(\mathbf{0}, \sigma_0^2 \mathbf{I}_K)$, $\mathbf{A} = (\mathbf{a}_1; \dots; \mathbf{a}_K)$ is a $K \times K$ matrix with \mathbf{a}_i being the i^{th} basis function ($K \times 1$ vector) specified later, and $\mathbf{v}(\cdot) = (v_1(\cdot), \dots, v_K(\cdot))^T$. As shown in Figure 1, the correlation of the methylation levels at nearby CpG sites decays as the genomic distance increases. This motivates us to model each weight function $v_i(\cdot)$ independently as a zero mean GaSP

$$v_i(\cdot) \sim \text{GaSP}(0, \sigma_i^2 c_i(\cdot, \cdot)), \quad (2)$$

where σ_i^2 is an unknown variance parameter and $c_i(\cdot, \cdot)$ is the correlation between sites. One popular choice of the correlation function is the Matérn kernel

$$c_i(d) = \frac{1}{2^{\nu_i-1} \Gamma(\nu_i)} \left(\frac{d}{\gamma_i} \right)^{\nu_i} \mathcal{K}_{\nu_i} \left(\frac{d}{\gamma_i} \right), \quad (3)$$

where $\Gamma(\cdot)$ is the gamma function, $\mathcal{K}_{\nu_i}(\cdot)$ is the modified Bessel function of the second kind with a roughness parameter ν_i , γ_i is a range parameter, and $d = |s_a - s_b|$ for any $s_a, s_b \in \mathcal{S}$. The roughness parameter of the Matérn kernel controls how smooth the stochastic process is. When $\nu_i = (2m_i + 1)/2$ with $m_i \in \mathbb{N}$, the GaSP with a Matérn kernel is m_i^{th} sample path differentiable and the Matérn kernel has a closed form expression in these scenarios. For instance, the exponential kernel is equivalent to the Matérn kernel with $\nu_i = 1/2$ and the Gaussian kernel is the Matérn kernel with $\nu_i \rightarrow +\infty$. The flexibility of the Matérn kernel makes it widely applicable for modeling spatially correlated data (Gelfand et al., 2010).

Denote $\mathbf{Y}(\mathbf{s}^{\mathcal{S}}) = (\mathbf{y}(\mathbf{s}^{\mathcal{S}})^T; \mathbf{y}^*(\mathbf{s}^{\mathcal{S}})^T)^T$. Following Higdon et al. (2008), we apply the singular value decomposition (SVD) to $\mathbf{Y}(\mathbf{s}^{\mathcal{S}}) = \mathbf{UDV}$ and estimate \mathbf{A} as $\mathbf{A} = \mathbf{UD}/\sqrt{n}$, for

the following reasons. First of all, the computational order of estimating \mathbf{A} is linear to n , which is essential when n is at the size of 10^6 . Secondly, we have $\mathbf{a}_i^T \mathbf{a}_j = 0$ if $i \neq j$, and hence $\mathbf{A}^T \mathbf{A}$ is a diagonal matrix, which substantially simplifies the computation of the likelihood. Moreover, $\mathbf{A} \mathbf{A}^T = \mathbf{Y}(\mathbf{s}^{\mathcal{J}}) \mathbf{Y}(\mathbf{s}^{\mathcal{J}})^T / n$, unifying the linear regression model under the framework of the nonseparable model shown later in Remark 1 of Section 4.

One can marginalize out the $K \times n$ weight matrix $\mathbf{v}(\mathbf{s}^{\mathcal{J}})$ explicitly for computing the likelihood. We first vectorize outputs $\mathbf{Y}_v(\mathbf{s}^{\mathcal{J}}) := \text{vec}(\mathbf{Y}(\mathbf{s}^{\mathcal{J}}))$ and weight matrix $\mathbf{v}_v(\mathbf{s}^{\mathcal{J}}) := \text{vec}(\mathbf{v}(\mathbf{s}^{\mathcal{J}})^T)$, both of which are Kn -dimensional vectors. Define a $Kn \times Kn$ matrix $\mathbf{A}_v := [\mathbf{I}_n \otimes \mathbf{a}_1; \dots; \mathbf{I}_n \otimes \mathbf{a}_K]$. By simple algebra, model (1) can be written as

$$\mathbf{Y}_v(\mathbf{s}^{\mathcal{J}}) = \mathbf{A}_v \mathbf{v}_v(\mathbf{s}^{\mathcal{J}}) + \boldsymbol{\epsilon}_{0v}, \quad (4)$$

where $\boldsymbol{\epsilon}_{0v} \sim N(0, \sigma_0^2 \mathbf{I}_{nK})$ and $\mathbf{v}_v(\mathbf{s}^{\mathcal{J}}) \mid \sigma_1^2, \dots, \sigma_K^2, \mathbf{R}_1, \dots, \mathbf{R}_K \sim MN(\mathbf{0}, \boldsymbol{\Sigma}_v)$, with the (l, m) entry of the \mathbf{R}_i being $c_i(s_l^{\mathcal{J}}, s_m^{\mathcal{J}})$. Here $\boldsymbol{\Sigma}_v = \text{blkdiag}(\sigma_1^2 \mathbf{R}_1; \dots; \sigma_K^2 \mathbf{R}_K)$, where $\text{blkdiag}(\cdot)$ means the block diagonal matrix between sites, and \mathbf{R}_i is the i^{th} correlation matrix, $i = 1, \dots, K$. As shown in Higdon et al. (2008), directly marginalizing out $\mathbf{v}_v(\mathbf{s}^{\mathcal{J}})$ leads to the sampling model, $\mathbf{Y}_v(\mathbf{s}^{\mathcal{J}}) \mid \sigma_0^2, \sigma_1^2, \dots, \sigma_K^2, \mathbf{R}_1, \dots, \mathbf{R}_K \sim \mathcal{MN}(\mathbf{0}, \mathbf{A}_v \boldsymbol{\Sigma}_v \mathbf{A}_v^T + \sigma_0^2 \mathbf{I}_{Kn})$. The straightforward computation of the likelihood, however, requires to evaluate the inverse of a $Kn \times Kn$ covariance matrix $\mathbf{A}_v \boldsymbol{\Sigma}_v \mathbf{A}_v^T + \sigma_0^2 \mathbf{I}_{Kn}$, which is computationally infeasible. We have the following lemma to ease the computational challenge.

Lemma 1. *Assume $\mathbf{A} = \mathbf{U} \mathbf{D} / \sqrt{n}$ and $\mathbf{Y}(\mathbf{s}^{\mathcal{J}}) = \mathbf{U} \mathbf{D} \mathbf{V}$ as the SVD decomposition. After integrating out $\mathbf{v}(\mathbf{s}^{\mathcal{J}})$, the marginal likelihood of $\mathbf{Y}(\mathbf{s}^{\mathcal{J}})$ in model (1) follows a product of K independent multivariate normal distributions,*

$$p(\mathbf{Y}(\mathbf{s}^{\mathcal{J}}) \mid \sigma_0^2, \sigma_1^2, \dots, \sigma_K^2, \mathbf{R}_1, \dots, \mathbf{R}_K) = |\mathbf{A}_v^T \mathbf{A}_v|^{-1/2} \prod_{i=1}^K p_{MN}(\hat{\mathbf{v}}_i(\mathbf{s}^{\mathcal{J}}); \mathbf{0}, \sigma_i^2 \mathbf{R}_i + \sigma_0^2 (\mathbf{a}_i^T \mathbf{a}_i)^{-1} \mathbf{I}_n), \quad (5)$$

where $p_{MN}(\cdot; \boldsymbol{\mu}, \boldsymbol{\Sigma})$ denotes the multivariate normal density with mean $\boldsymbol{\mu}$ and covariance $\boldsymbol{\Sigma}$, $\hat{\mathbf{v}}_i(\mathbf{s}^{\mathcal{D}})$ is the transpose of the i^{th} row of $\hat{\mathbf{v}}(\mathbf{s}^{\mathcal{D}}) = (\mathbf{A}^T \mathbf{A})^{-1} \mathbf{A}^T \mathbf{Y}(\mathbf{s}^{\mathcal{D}})$.

Lemma 1 states that the marginal likelihood by model (1) can be written as a product of K multivariate normal densities, which simplifies the computation. In particular, instead of computing the multivariate normal densities with a $Kn \times Kn$ covariance matrix, one can evaluate the densities by K independent multivariate normal distributions, each of which has an $n \times n$ covariance matrix. The direct computation of the inverse of an $n \times n$ covariance matrix, however, is still very hard in general, when n is at the size of 10^6 . An efficient algorithm that computes the exact likelihood will be provided in Section 3.

The goal of imputation is to find the predictive distribution at an unexamined site s_j^* conditioning on the available data. Denote $\mathbf{Y}(s_j^*) = (\mathbf{y}(s_j^*)^T; \mathbf{y}^*(s_j^*)^T)^T$, where $\mathbf{y}(s_j^*)$ and $\mathbf{y}^*(s_j^*)$ are the j^{th} column of $\mathbf{y}(\mathbf{s}^*)$ and $\mathbf{y}^*(\mathbf{s}^*)$ respectively. We have the following lemma.

Lemma 2. *We assume the same conditions in Lemma 1.*

1. For every s_j^* , one has

$$\mathbf{Y}(s_j^*) \mid \mathbf{Y}(\mathbf{s}^{\mathcal{D}}), \sigma_{0:K}^2, \boldsymbol{\gamma}_{1:K} \sim MN \left(\hat{\boldsymbol{\mu}}(s_j^*), \hat{\boldsymbol{\Sigma}}(s_j^*) \right).$$

Here $\hat{\boldsymbol{\mu}}(s_j^*) = \mathbf{A} \hat{\mathbf{v}}^*(s_j^*)$ and $\hat{\boldsymbol{\Sigma}}(s_j^*) = \mathbf{A} \mathbf{D}^*(s_j^*) \mathbf{A}^T + \sigma_0^2 \mathbf{I}_K$, where $\hat{\mathbf{v}}^*(s_j^*) = (\hat{v}_1^*(s_j^*), \dots, \hat{v}_K^*(s_j^*))^T$ with $\hat{v}_i^*(s_j^*) = \mathbf{r}_i^T(s_j^*) (\mathbf{R}_i + \frac{\sigma_0^2 (\mathbf{a}_i^T \mathbf{a}_i)^{-1}}{\sigma_i^2} \mathbf{I}_n)^{-1} \hat{\mathbf{v}}_i(\mathbf{s}^{\mathcal{D}})$ and $\hat{\mathbf{v}}_i(\mathbf{s}^{\mathcal{D}})$ being the transpose of the i^{th} row of $\hat{\mathbf{v}}(\mathbf{s}^{\mathcal{D}})$, $\mathbf{r}_i(s_j^*) = (c_i(s_j^*, s_1^{\mathcal{D}}), \dots, c_i(s_j^*, s_n^{\mathcal{D}}))^T$, $\mathbf{D}^*(s_j^*)$ is a diagonal matrix with $\sigma_i^2 c_i^*(s_j^*)$ as the i^{th} diagonal term and $c_i^*(s_j^*) = c_i(s_j^*, s_j^*) - \mathbf{r}_i^T(s_j^*) (\mathbf{R}_i + \frac{\sigma_0^2 (\mathbf{a}_i^T \mathbf{a}_i)^{-1}}{\sigma_i^2} \mathbf{I}_n)^{-1} \mathbf{r}_i(s_j^*)$.

2. Denote the partition $\hat{\boldsymbol{\mu}}(s_j^*) = (\hat{\boldsymbol{\mu}}_0^T(s_j^*), \hat{\boldsymbol{\mu}}_*^T(s_j^*))^T$ and $\hat{\boldsymbol{\Sigma}}(s_j^*) = \begin{pmatrix} \hat{\boldsymbol{\Sigma}}_{00}(s_j^*) & \hat{\boldsymbol{\Sigma}}_{0*}(s_j^*) \\ \hat{\boldsymbol{\Sigma}}_{*0}(s_j^*) & \hat{\boldsymbol{\Sigma}}_{**}(s_j^*) \end{pmatrix}$.

For every s_j^* , the predictive distribution of the unobserved $\mathbf{y}^*(s_j^*)$ follows

$$\mathbf{y}^*(s_j^*) \mid \mathbf{y}(\mathbf{s}^{\mathcal{D}}), \mathbf{y}(\mathbf{s}^*), \mathbf{y}^*(\mathbf{s}^{\mathcal{D}}), \sigma_{0:K}^2, \boldsymbol{\gamma}_{1:K} \sim MN \left(\hat{\boldsymbol{\mu}}_{*|0}(s_j^*), \hat{\boldsymbol{\Sigma}}_{*|0}(s_j^*) \right),$$

where $\hat{\boldsymbol{\mu}}_{*|0}(s_j^*) = \hat{\boldsymbol{\mu}}_*(s_j^*) + \hat{\boldsymbol{\Sigma}}_{*0}(s_j^*)\hat{\boldsymbol{\Sigma}}_{00}^{-1}(s_j^*) (\mathbf{y}(s_j^*) - \hat{\boldsymbol{\mu}}_0(s_j^*))$ and $\hat{\boldsymbol{\Sigma}}_{*|0}(s_j^*) = \hat{\boldsymbol{\Sigma}}_{**}(s_j^*) - \hat{\boldsymbol{\Sigma}}_{*0}(s_j^*)\hat{\boldsymbol{\Sigma}}_{00}^{-1}(s_j^*)\hat{\boldsymbol{\Sigma}}_{0*}(s_j^*)$.

In the methylation levels imputation study, $\hat{\boldsymbol{\mu}}_{*|0}(s_j^*)$ can be used as predictions for $\mathbf{y}^*(s_j^*)$ for any site s_j^* , by properly conditional on all observations.

2.2 Nonseparable GaSP model with heterogeneous noises

The nonseparable model (1) assumes a shared noise parameter σ_0^2 , which is typically very restrictive. We generalize the model by assuming different noise parameters as follows

$$\begin{aligned} \mathbf{Y}(s) &= \mathbf{A}\tilde{\mathbf{v}}(s) + \boldsymbol{\epsilon}_0, \\ \tilde{v}_i(\cdot) &= v_i(\cdot) + \epsilon_i, \quad i = 1, \dots, K, \end{aligned} \tag{6}$$

with $\boldsymbol{\epsilon}_0 \sim N(0, \sigma_0^2 \mathbf{I}_K)$ for any $s \in \mathcal{S}$, each weight function $v_i(\cdot)$ being assumed the same as the previous independent GaSP in (2) and ϵ_i being an independent zero-mean Gaussian noise with variance τ_i . We still assume $\mathbf{A} = \mathbf{U}\mathbf{D}/\sqrt{n}$ where \mathbf{U} and \mathbf{D} are defined through the SVD decomposition of $\mathbf{Y}(\mathbf{s}^{\mathcal{S}})$. In model (6), $\tilde{v}_i(\cdot)$ follows a zero-mean GaSP with noise

$$\tilde{v}_i(\cdot) \sim \text{GaSP}(0, \sigma_i^2 \tilde{c}_i(\cdot, \cdot)), \tag{7}$$

with the covariance $\sigma_i^2 \tilde{c}_i(s_a, s_b) = \sigma_i^2 (c_i(s_a, s_b) + \eta_i \mathbf{1}_{a=b})$, where $\eta_i = \tau_i/\sigma_i^2$ is the nugget-variance ratio and $c_i(\cdot, \cdot)$ is defined in (3) with a fixed ν_i and an unknown range parameter γ_i , for $i = 1, \dots, K$. Replacing \mathbf{R}_i with $\tilde{\mathbf{R}}_i = \mathbf{R}_i + \eta_i \mathbf{I}_n$ in Lemma 1, the marginal likelihood of $\mathbf{Y}(\mathbf{s}^{\mathcal{S}})$ can be written as a product of K independent multivariate normal densities,

$$p(\mathbf{Y}(\mathbf{s}^{\mathcal{S}}) | \sigma_{1:K}^2, \eta_{1:K}, \gamma_{1:K}) = |\mathbf{A}_v^T \mathbf{A}_v|^{-1/2} \prod_{i=1}^K p_{MN}(\hat{\mathbf{v}}_i(\mathbf{s}^{\mathcal{S}}); \mathbf{0}, \sigma_i^2 \tilde{\mathbf{R}}_i + \sigma_0^2 (\mathbf{a}_i^T \mathbf{a}_i)^{-1} \mathbf{I}_n), \tag{8}$$

where $\hat{\mathbf{v}}_i(\mathbf{s}^{\mathcal{D}})$ is the transpose of the i^{th} row of $\hat{\mathbf{v}}(\mathbf{s}^{\mathcal{D}}) = (\mathbf{A}^T \mathbf{A})^{-1} \mathbf{A}^T \mathbf{Y}(\mathbf{s}^{\mathcal{D}})$. The marginal likelihood in (5) is a special case of the marginal likelihood in (8) when $\eta_i = 0$ for $i = 1, \dots, K$. Note that the above model is not identifiable between η_1, \dots, η_K , and σ_0^2 . In the following, we simply constrain $\sigma_0^2 = 0$ to avoid the potential identifiability issue.

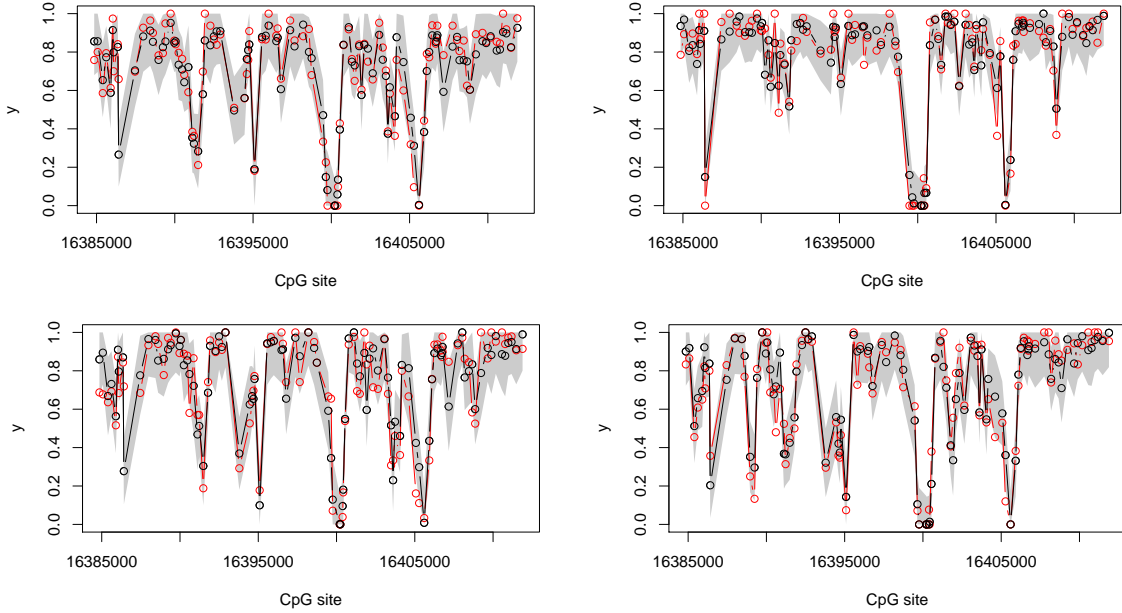


Figure 2: The held-out methylation levels (red circles) and prediction of methylation levels (black circles) by the nonseparable GaSP model for randomly selected 4 samples at 100 CpG sites. The 95% posterior predictive interval is dashed as the shaded area.

The predictive distributions of model (6) at unobserved CpG sites takes almost the same form in Lemma 2 by replacing \mathbf{R}_i and $c_i(\cdot, \cdot)$ with $\tilde{\mathbf{R}}_i$ and $\tilde{c}_i(\cdot, \cdot)$ respectively. Figure 2 plots the predicted methylation levels as the black circles at 100 held-out CpG sites for 4 samples, with the examined methylation levels marked as the red circles. The prediction by the nonseparable GaSP model captures the pattern of the methylation levels reasonably well, with an adequate length of 95% predictive interval, graphed as the shaded area. A more detailed comparison between the nonseparable GaSP model and other computational feasible alternatives is given in Section 5.

3 Computational strategy

The computations of the likelihood in model (6) require to compute the inverse of \mathbf{R}_i , each with $O(n^3)$ operations, making the implementation impractical when n is large. We introduce a computationally efficient algorithm, based on the connection between the Gaussian random field and Gaussian Markov random field (GMRF). The idea is introduced in Whittle (1954, 1963); Hartikainen and Sarkka (2010), where the Matérn covariance was shown to be Markov. Unlike many other methods, no approximation to the likelihood is needed in this approach. We briefly review this computational strategy and extend it to compute the exact likelihood of the nonseparable GaSP model with linear operations.

Consider a continuous auto-regressive model with order p , defined by a stochastic differential equation (SDE),

$$c_p f^{(p)}(s) + c_{p-1} f^{(p-1)}(s) + \dots + c_0 f(s) = b_0 z(s), \quad (9)$$

where $f^{(l)}(s)$ is the l^{th} derivative of $f(s)$ and $z(s)$ is the standard Gaussian white noise process defined on $s \in \mathbb{R}$. Here we set $c_p = 1$ to avoid the nonidentifiability issue. The spectral density of equation (9) is $S_{\mathbb{R}}(t) = \frac{b_0^2}{|C(2\pi it)|^2}$, where i is the imaginary number, and the operator $C(\cdot)$ is defined by $C(z) = \sum_{l=0}^p c_l z^l$. The form of the above spectral density is $S_{\mathbb{R}}(t) = \frac{\text{constant}}{\text{polynomial in } t^2}$, which is a rational functional form. It has been shown in Whittle (1954, 1963) that the spectral density of GaSP with the Matérn covariance is

$$S_{Mat}(t) \propto \frac{1}{(\lambda^2 + t^2)^{(\nu+1/2)}}, \quad (10)$$

where $\lambda = \frac{\sqrt{2\nu}}{\gamma}$ with the range parameter γ and the roughness parameter ν . The spectral density in (10) follows a rational functional form, meaning that we can utilize the GMRF representation for computation, elaborated in the following subsection.

3.1 The computation by continuous time stochastic process

Here we assume the Matérn kernel with $\nu = 5/2$ as for the demonstration purpose

$$c(d) = \left(1 + \frac{\sqrt{5}d}{\gamma} + \frac{5d^2}{3\gamma^2}\right) \exp\left(-\frac{\sqrt{5}d}{\gamma}\right), \quad (11)$$

with $d = |s_a - s_b|$ for any $s_a, s_b \in \mathcal{S}$. The computational advantages introduced in this subsection hold for Matérn kernel with $\nu = (2m + 1)/2$ for all $m \in \mathbb{N}$.

As shown in (8), the likelihood of $\mathbf{Y}(\mathbf{s}^{\mathcal{S}})$ in model (6) with $\sigma_0^2 = 0$ can be written in terms of $\tilde{\mathbf{v}}(\mathbf{s}^{\mathcal{S}}) = (\mathbf{A}^T \mathbf{A})^{-1} \mathbf{A}^T \mathbf{Y}(\mathbf{s}^{\mathcal{S}})$. We thus focus on discussing the likelihood of $\tilde{\mathbf{v}}(\mathbf{s}^{\mathcal{S}})$. The nonseparable GaSP model in (6) with $\sigma_0^2 = 0$ can be represented as

$$\begin{aligned} \tilde{v}_i(\cdot) &= f_i(\cdot) + \epsilon_i, \\ f_i(\cdot) &\sim \text{GaSP}(0, \sigma_i^2 c_i(\cdot, \cdot)), \end{aligned} \quad (12)$$

where $\epsilon_i \sim \mathcal{N}(0, \tau_i)$ being an independent noise with $\tau_i = \sigma_i^2 \eta_i$, for $1 \leq i \leq K$. Denote $\boldsymbol{\theta}_i(s) := (f_i(s), f_i^{(1)}(s), f_i^{(2)}(s))^T$, where $f_i^{(l)}(s)$ is the l^{th} derivative of $f_i(s)$ with regard to s , $l = 1, 2$. For each $i = 1, \dots, K$, GaSP with the correlation defined in (11) follows an SDE

$$\frac{d\boldsymbol{\theta}_i(s)}{ds} = \mathbf{J}_i \boldsymbol{\theta}_i(s) + \mathbf{L} z_i(s),$$

where $z_i(s)$ is a zero-mean Gaussian white noise process with variance σ_i^2 and $\lambda_i = \sqrt{2\nu_i}/\gamma_i$. The closed form expression of \mathbf{J}_i and \mathbf{L} is given in the Appendix B. Denote $q_i = \frac{16}{3} \sigma_i^2 \lambda_i^5$ and $\mathbf{F} = (1, 0, 0)$. The solution of the above SDE can be represented explicitly as

$$\begin{aligned} \tilde{v}_i(s_{j+1}) &= \mathbf{F} \boldsymbol{\theta}_i(s_{j+1}) + \epsilon_i, \\ \boldsymbol{\theta}_i(s_{j+1}) &= \mathbf{G}_i(s_j) \boldsymbol{\theta}_i(s_j) + \mathbf{W}_i(s_j) \\ \mathbf{W}_i(s_j) &\sim N(0, \mathbf{Q}_i(s_j)) \end{aligned} \quad (13)$$

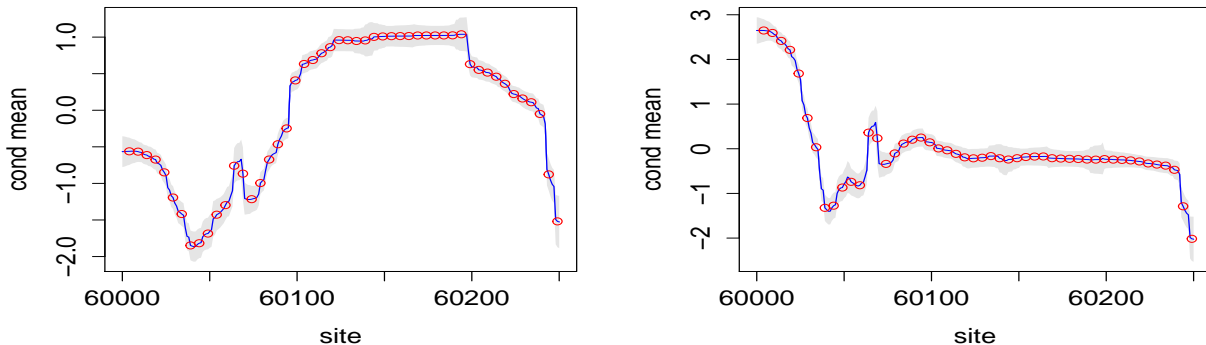


Figure 3: Comparison of the computation of the GaSP likelihood from the direct inversion of the covariance and FFBS algorithm. The blue curves are the posterior mean of $\tilde{\mathbf{v}}_i(\mathbf{s}^*) | \tilde{\mathbf{v}}_i(\mathbf{s}^{\mathcal{D}})$ by equation (13) and the shaded area is the 95% posterior predictive interval of the mean function at a small region for $i = 1$ (left panel) and $i = 2$ (right panel), for a given set of parameters $(\sigma_i^2, \gamma_i, \tau_i)$. The red dots are the posterior mean $\tilde{\mathbf{v}}_i(\mathbf{s}_j^*) | \tilde{\mathbf{v}}_i(\mathbf{s}^{\mathcal{D}})$ of 50 s_j^* at the same region with the same set of parameters by the direct computation for the GaSP model. The root of mean square errors (RMSE) between the blue curves and red circles at these 50 s_j^* are 2.04×10^{-13} and 2.41×10^{-12} for the left panel and right panel respectively.

where $\mathbf{G}_i(s_j) = e^{\mathbf{J}_i(s_{j+1}-s_j)}$ and $\mathbf{Q}_i(s_j) = \int_0^{s_{j+1}-s_j} e^{\mathbf{J}_i t} \mathbf{L} q_i \mathbf{L}^T e^{\mathbf{J}_i^T t} dt$ for $j = 1, \dots, n-1$. The stationary distribution of $\boldsymbol{\theta}_i$ is $\boldsymbol{\theta}_i(s_0) \sim MN(0, \mathbf{Q}_i(s_0))$, with $\mathbf{Q}_i(s_0) = \int_0^\infty e^{\mathbf{J}_i t} \mathbf{L} q_i \mathbf{L}^T e^{\mathbf{J}_i^T t} dt$. All $\mathbf{G}_i(s_j)$, $\mathbf{Q}_i(s_j)$, $\mathbf{Q}_i(s_0)$, and the likelihood of $\boldsymbol{\theta}_i$ are derived in the supplementary materials.

With the above setup, the posterior for $\boldsymbol{\theta}_i(s)$, $i = 1, \dots, K$, can be computed by a forward filtering and backward sampling/smoothing (FFBS) algorithm (West and Harrison, 1997; Petris et al., 2009), which only requires $O(n)$ computational operations, a lot smaller than $O(n^3)$ operations in the direct computation of the GaSP model. The prediction at \mathbf{s}^* also only requires linear computational operations to the number of sites, so the total computational operations are only $O(N)$ altogether. Furthermore, $\boldsymbol{\theta}_i(s)$ can be explicitly marginalized out for all s instead of the posterior sampling, discussed in Section 3.2.

Figure 3 compares the posterior means of $\tilde{\mathbf{v}}_i(\mathbf{s}^*) | \tilde{\mathbf{v}}_i(\mathbf{s}^{\mathcal{D}})$ by the FFBS algorithm and direct computation of GaSP for some s_j^* given set of parameters. Since they are the same quantities computed in two different ways, the difference only depends on the machine pre-

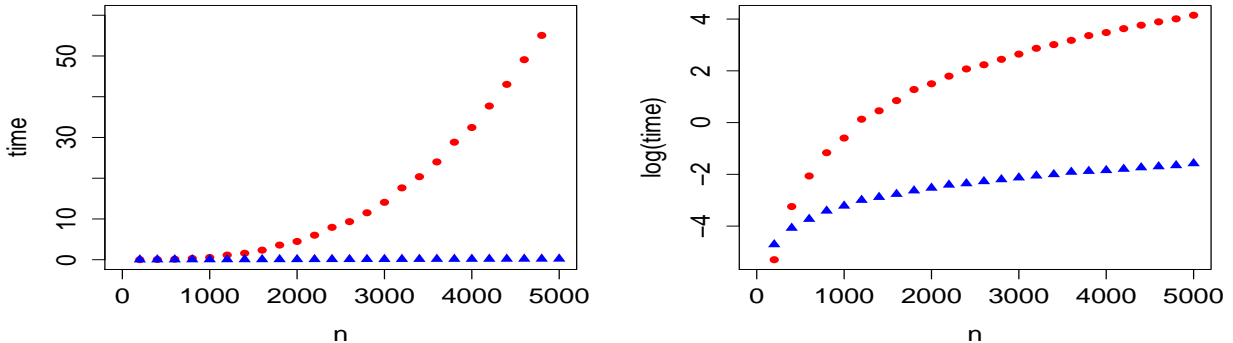


Figure 4: Computational time in seconds for one evaluation of the likelihood with the normal scale (left panel) and log scale (right panel). The red dot represents the computational time by the direct computation and blue solid triangle is by the FFBS algorithm.

cision, which is extremely small. The main advantage of our method is that all summary statistics of interest, such as the posterior predictive mean and variance, as well as the marginal likelihood can be computed exactly.

The computational time between them, however, differs significantly. As shown in Figure 4, the computation by the FFBS algorithm is a lot more efficient than the direct evaluation of the likelihood, which requires $O(n^3)$ for matrix inversion. For instance, when $n = 5,000$, evaluating the likelihood by the FFBS algorithm only takes around 0.1 second on a laptop, while the direct computation takes around 60 seconds.

Note when $\nu_i = 5/2$, the Matérn covariance matrix in (11) and its inversion are both dense $n \times n$ matrices with rank n . However, the covariance matrix of the latent states, $\boldsymbol{\theta}_i(s) = (f_i(s), f_i^{(1)}(s), f_i^{(2)}(s))^T$ is sparse, as shown in supplementary materials. The result holds for all Matérn classes when $\nu_i = (2m + 1)/2$, with $m \in \mathbb{N}$.

3.2 Parameter estimation

The most computationally intensive part of the FFBS algorithm is to sample $3Kn$ latent states $\boldsymbol{\theta}_i(s_j)$ for $i = 1, \dots, K$ and $j = 1, \dots, n$. Fortunately, one can avoid it by marginalizing

out the latent states explicitly,

$$p(\tilde{\mathbf{v}}(\mathbf{s}^{\mathcal{D}})|\boldsymbol{\sigma}_{1:K}^2, \boldsymbol{\tau}_{1:K}, \boldsymbol{\gamma}_{1:K}) = \prod_{i=1}^K \left\{ p(\tilde{v}_i(s_1^{\mathcal{D}})|\sigma_i^2, \tau_i, \gamma_i) \prod_{j=2}^n p(\tilde{v}_i(s_j^{\mathcal{D}})|\tilde{v}_i(\mathbf{s}_{1:j-1}^{\mathcal{D}}), \sigma_i, \tau_i, \gamma_i) \right\},$$

each term of which follows a normal distribution given in the one-step look ahead prediction in the FFBS algorithm (West and Harrison, 1997). The marginal likelihood $p(\tilde{\mathbf{v}}(\mathbf{s}^{\mathcal{D}})|\gamma_i, \eta_i, \sigma_i^2)$ can also be computed with linear computational operations in terms of n , allowing us to evaluate the likelihood without making an approximation.

To complete the model, we assume the prior as follows,

$$\pi(\boldsymbol{\sigma}_{1:K}^2, \boldsymbol{\tau}_{1:K}, \boldsymbol{\gamma}_{1:K}) \propto \prod_{i=1}^K \frac{\pi(\tau_i, \gamma_i)}{\sigma_i^2}. \quad (14)$$

Denote $\zeta_i := 1/\gamma_i$ and $\eta_i := \tau_i/\sigma_i^2$. We assume the jointly robust prior (Gu, 2016; Gu et al., 2018) for the transformed parameters $\pi(\zeta_i, \eta_i) \propto (C_i\zeta_i + \eta_i)^{a_i} \exp(-b_i(C_i\zeta_i + \eta_i))$, for $i = 1, \dots, K$, where C_i , a_i and b_i are prior parameters. This prior approximates the reference prior in tail rates and is robust for posterior mode estimation (Gu et al., 2017). For the prior parameter, we use the default choice $a = 1/2$, $b = 1$, and $C_i = |\mathcal{S}|/n$, where $|\mathcal{S}|$ is the length of \mathcal{S} .

As n is large, the Markov chain Monte Carlo (MCMC) algorithm is still very slow for sampling the posterior distribution. We estimate the parameters by the posterior mode,

$$(\hat{\zeta}_i, \hat{\eta}_i) = \underset{\zeta_i, \eta_i}{\operatorname{argmax}} \{p(\tilde{\mathbf{v}}(\mathbf{s}^{\mathcal{D}})|\zeta_i, \eta_i)\pi(\zeta_i, \eta_i)\}. \quad (15)$$

The posterior mode of the variance parameters is $\hat{\sigma}_i^2 = S_i^2/(n+1)$ with $S_i^2 = \tilde{\mathbf{v}}_i^T(\mathbf{s}^{\mathcal{D}})\tilde{\mathbf{R}}_i^{-1}\tilde{\mathbf{v}}_i^T(\mathbf{s}^{\mathcal{D}})$. The posterior mean and MLE of σ_i^2 are $S_i^2/(n-1)$ and S_i^2/n , respectively. When n is large, these estimations are almost the same.

4 Unification of linear regression, separable model and nonseparable model

In this section, we show the linear regression model that was used for methylation level imputation (Zhang et al., 2015), and the separable GaSP model used in computer model emulation (Conti and O’Hagan (2010); Gu and Berger (2016)) are both special cases of the nonseparable GaSP model introduced in Section 2.

4.1 Linear regression strategies

Assuming that the samples are independent to each other, a simple model is to apply the linear regression separately for each CpG site s_j , $j = 1, \dots, N$, as follows,

$$y_i(s_j) = \mathbf{H}_i(s_j)\boldsymbol{\beta}_j + \epsilon_{ij}, i = 1, \dots, K, \tag{16}$$

where $\mathbf{H}_i(s_j)$ are the covariates for the j^{th} CpG site of the i^{th} sample and $\epsilon_{ij} \sim N(0, \sigma_{0j}^2)$ is an independent mean-zero Gaussian noise. In Zhang et al. (2015), some site-specific features, such as methylation levels at nearby CpG sites, are used as covariates for imputation. This approach assumes that methylation levels are independent across samples at every CpG site. However, methylation levels of different samples at a CpG site are generally correlated, as shown in Figure 1. Numerical results will be shown that exploiting the correlation between samples leads to drastic improvement in imputation in Section 5.

Alternatively, a regression model that exploits the correlations across samples follows

$$y_i(s_j) = \mathbf{H}_i(s_j)\boldsymbol{\beta}_i + \epsilon_{ij}, j = 1, \dots, N, \tag{17}$$

with $\epsilon_{ij} \sim N(0, \sigma_{i0}^2)$. Here each site is treated independently. Assume the methylation levels

were first centered to have a zero mean and let $\mathbf{H}_i(s_j) = (y_1(s_j), \dots, y_k(s_j))$, meaning only the methylation levels of the k samples with full observations are used as covariates, the model for $\mathbf{s}^{\mathcal{D}}$ can be expressed $\mathbf{y}_i^*(\mathbf{s}^{\mathcal{D}})^T = \mathbf{y}(\mathbf{s}^{\mathcal{D}})^T \boldsymbol{\beta}_i + \boldsymbol{\epsilon}_i$, where $\mathbf{y}_i^*(\mathbf{s}^{\mathcal{D}})$ is the i^{th} row of $\mathbf{y}^*(\mathbf{s}^{\mathcal{D}})$ and $\boldsymbol{\epsilon}_i \sim N(0, \sigma_{i0}^2 \mathbf{I}_n)$. The least squares (LS) estimator of $\boldsymbol{\beta}_i$ is $\hat{\boldsymbol{\beta}}_i = \{\mathbf{y}(\mathbf{s}^{\mathcal{D}}) \mathbf{y}(\mathbf{s}^{\mathcal{D}})^T\}^{-1} \mathbf{y}(\mathbf{s}^{\mathcal{D}}) \mathbf{y}_i^*(\mathbf{s}^{\mathcal{D}})^T$, where $\mathbf{y}_i^*(\mathbf{s}^{\mathcal{D}}) = (y_i^*(\mathbf{s}_1^{\mathcal{D}}), \dots, y_i^*(\mathbf{s}_n^{\mathcal{D}}))$ being the i^{th} row of $\mathbf{y}^*(\mathbf{s}^{\mathcal{D}})$. The predictive mean of the methylation level of the i^{th} sample at the j^{th} unexamined site, $\mathbf{H}_i(s_j^*) \hat{\boldsymbol{\beta}}_i$, follows

$$\mathbb{E}[\mathbf{y}_i^*(s_j^*) \mid \mathbf{y}(\mathbf{s}^{\mathcal{D}}), \mathbf{y}^*(\mathbf{s}^{\mathcal{D}}), \mathbf{y}(\mathbf{s}^*), \hat{\boldsymbol{\beta}}_i] = \mathbf{y}(s_j^*)^T \{\mathbf{y}(\mathbf{s}^{\mathcal{D}}) \mathbf{y}(\mathbf{s}^{\mathcal{D}})^T\}^{-1} \mathbf{y}(\mathbf{s}^{\mathcal{D}}) \mathbf{y}_i^*(\mathbf{s}^{\mathcal{D}})^T, \quad (18)$$

with $\mathbf{y}(s_j^*) = (y_1(s_j^*), \dots, y_k(s_j^*))^T$ being the j^{th} column of $\mathbf{y}(\mathbf{s}^*)$, for $i = 1, \dots, k^*$, $j = 1, \dots, n^*$. The following remark establishes the connection between the linear regression and nonseparable GaSP model.

Remark 1. *The predictive mean under the linear regression model in (18) is identical to the predictive mean $\hat{\boldsymbol{\mu}}_{*|0}(s_j^*)$ of the nonseparable model with $\sigma_0^2 = 0$ in Lemma 2 if in model (1),*

- (i.) $\mathbf{A} = \mathbf{U}\mathbf{D}/\sqrt{n}$, where \mathbf{U} and \mathbf{D} are defined through the SVD decomposition of $\mathbf{Y}(\mathbf{s}^{\mathcal{D}})$.
- (ii.) $v_i(\cdot)$ is the realization of independent mean zero Gaussian noise with the same variance.

4.2 Separable model

Denote \mathbf{Y} as a $K \times N$ matrix where each row is a sample of methylation levels at N CpG sites. Compared to the regression models, the following joint model is sometimes preferred

$$\mathbf{Y} = \mathbf{Z} + \boldsymbol{\epsilon}_0, \quad (19)$$

where $\boldsymbol{\epsilon}_0$ is a zero-mean independent noise and \mathbf{Z} is a $K \times N$ random matrix modeled from a matrix-variate normal distribution, $\mathbf{Z} \sim N_{K,N}(\boldsymbol{\mu}, \boldsymbol{\Sigma}, \boldsymbol{\Lambda})$, with a $K \times N$ mean matrix $\boldsymbol{\mu}$, a $K \times K$ row covariance matrix $\boldsymbol{\Sigma}$, and an $N \times N$ column correlation matrix $\boldsymbol{\Lambda}$.

We call model (19) *the separable model*, as the correlations across samples and across sites are expressed separately by Σ and Λ respectively. Assuming that Λ is modeled by a correlation function, where the (i, j) entry $\Lambda_{i,j} = c(d)$, with $c(\cdot)$ being the correlation function. The following remark states the separable model defined in (19) is a special case of the nonseparable model in (1).

Remark 2. *If $\mu = \mathbf{0}$, the separable model defined in (19) is equivalent to the nonseparable GaSP model in (1) if*

(i.) \mathbf{A} is chosen such that $\Sigma = \mathbf{A}\mathbf{A}^T$.

(ii.) The covariance function in (2) has the unit variance and $c_i(d) = c(d)$, for $i = 1, \dots, K$.

5 Numerical comparison

We evaluate the nonseparable GaSP model in (6) and compare to several alternative methods: two linear regression strategies (by site in (16) and by sample in (17)), nearest neighborhood method (using only the observed methylation level closest to the unobserved site for prediction) and two regression strategies by random forest (Liaw and Wiener, 2002). We also introduce a localized Kriging method by partitioning the data into small blocks, and compare it with the nonseparable GaSP model in the supplementary materials.

The performance of these methods is evaluated on the out of sample prediction for WGBS data and Methylation450 data based on the following criteria

$$\begin{aligned}
 RMSE &= \sqrt{\frac{\sum_{i=1}^{k^*} \sum_{j=1}^{n^*} (\hat{y}_i^*(s_j^*) - y_i^*(s_j^*))^2}{k^*n^*}}, \\
 PCI(95\%) &= \frac{1}{k^*n^*} \sum_{i=1}^{k^*} \sum_{j=1}^{n^*} 1\{y_i^*(s_j^*) \in CI_{ij}(95\%)\}, \\
 LCI(95\%) &= \frac{1}{k^*n^*} \sum_{i=1}^{k^*} \sum_{j=1}^{n^*} \text{length}\{CI_{ij}(95\%)\},
 \end{aligned}$$

where for $1 \leq i \leq k^*$ and $1 \leq j \leq n^*$, $y_i^*(s_j^*)$ is the held-out methylation levels of the i^{th} sample at the j^{th} CpG site; $\hat{y}_i^*(s_j^*)$ is the predicted held-out methylation level of the i^{th} sample at the j^{th} CpG site; $CI_{ij}(95\%)$ is the 95% posterior credible interval; and $\text{length}\{CI_{ij}(95\%)\}$ is the length of the 95% posterior credible interval. An effective method is expected to have small out-of-sample RMSE, $P_{CI}(95\%)$ being close to nominal 95% level, and small $L_{CI}(95\%)$. In Zhang et al. (2015), a CpG site is defined to be methylated if more than 50% of the probes are methylated, and the accuracy rate of a method is defined by the proportion of the correct predictions of CpG sites being methylated or not. We also use the accuracy rate as a criterion to compare the nonseparable GaSP model and its competitors in the following numerical results.

5.1 Real dataset 1: WGBS data

We first compare the out-of-sample prediction of different methods using the criteria discussed above for roughly 10^6 methylation levels in the WGBS dataset. In this dataset, 24 samples are available in total and we randomly select $k^* = 4$ samples, whose methylation levels are partially observed (with certain proportion being held out), while the methylation levels of the rest of the samples are fully observed. We consider three scenarios, in which 50%, 75%, and 90% of the methylation levels of these 4 samples are held out as the test dataset. The methylation levels of each sample are centered and the mean is added back for prediction in the GaSP model (Higdon et al., 2008). We estimate the range and nugget parameters using equation (15) and rely on the predictive distribution of model (6) for combining different sources of information in prediction.

As shown in Table 1, the nonseparable GaSP model has the smallest out-of-sample RMSE, making it the most accurate in out-of-sample prediction in all scenarios. For instance, when 50% of CpG sites are held out, the nonseparable GaSP method improves the RMSE by at least 15% compared to any other methods we considered. The gain is from integrating the

50% held-out CpG sites	RMSE	$P_{CI}(95\%)$	$L_{CI}(95\%)$	Accuracy
Nonseparable GaSP	0.085	0.961	0.300	0.970
Nearest neighborhood	0.147	/	/	0.943
Linear model by site	0.100	0.913	0.261	0.966
Random forest by site	0.103	/	/	0.964
Linear model by sample	0.100	0.941	0.308	0.962
Random forest by sample	0.101	/	/	0.963
75% held-out CpG sites	RMSE	$P_{CI}(95\%)$	$L_{CI}(95\%)$	Accuracy
Nonseparable GaSP	0.089	0.961	0.309	0.968
Nearest neighborhood	0.166	/	/	0.934
Linear model by site	0.106	0.910	0.274	0.963
Random forest by site	0.108	/	/	0.962
Linear model by sample	0.100	0.941	0.308	0.962
Random forest by sample	0.097	/	/	0.964
90% held-out CpG sites	RMSE	$P_{CI}(95\%)$	$L_{CI}(95\%)$	Accuracy
Nonseparable GaSP	0.096	0.941	0.296	0.966
Nearest neighborhood	0.166	/	/	0.934
Linear model by site	0.114	0.908	0.289	0.959
Random forest by site	0.114	/	/	0.957
Linear model by sample	0.100	0.941	0.308	0.962
Random forest by sample	0.098	/	/	0.963

Table 1: Comparison of different methods for the WGBS data. From the upper to the lower, 25%, 50%, 75% and 90% of the first million methylation levels of $k^* = 4$ samples are held out for testing, respectively.

correlations between CpG sites and between samples through a coherent statistical model, while the other models only utilize partial information. For example, the methods in rows 2 to 4 only exploit the site-wise correlation by assuming the observations are independent across different samples at each CpG site, while the methods in rows 5 to 6 only exploit the correlation between samples.

When more and more data are held-out as the test data, the correlation between nearby observed methylation levels gets smaller as the average distance between two sites with observed methylation levels gets larger, making it harder for prediction. Yet the nonseparable GaSP model still results in the smallest RMSE, which is around 0.089 and 0.096, when 75% and 90% of CpG sites are held out respectively.

	RMSE	$P_{CI}(95\%)$	$L_{CI}(95\%)$	Accuracy
Nonseparable GaSP	0.030	0.972	0.122	0.991
Nearest neighborhood	0.150	/	/	0.944
Linear model by site	0.034	0.945	0.099	0.990
Random forest by site	0.034	/	/	0.990
Linear model by sample	0.031	0.957	0.106	0.990
Random forest by sample	0.031	/	/	0.990

Table 2: Comparison of different methods for the Methylation450K data. 20% CpG sites of the $k^* = 50$ people are held out for testing.

Furthermore, the nonseparable GaSP model produces 95% credible interval that covers approximately 95% of the held-out outcomes, with the comparatively short length of credible interval. In contrast, two linear regression models are over-confident, as the coverages are all below the nominal 95% level. This is not surprising, because the independence assumption by the linear models (either between sites or between samples) makes the likelihood too concentrated. Consequently, the predictive interval by the linear model is typically too narrow to cover the held-out samples as it claims, while the likelihood of the nonseparable GaSP model describes the complicated patterns of correlation better, thereby presenting an adequate predictive credible interval.

The nonseparable GaSP also leads to around 97% accuracy in predicting whether a CpG site is methylated or not (equivalently predicting whether more than half of the probes are methylated in the held-out CpG sites), which is also the highest compared to all other methods. Note the differences between the nonseparable model and other methods are small, as around 90% of the CpG sites are methylated in this dataset, and thus a benchmark estimator could achieve at least 90% accuracy in prediction.

5.2 Real dataset 2: Methylation450 data

In this section, we study the numerical performance of all the methods for the Methy450K dataset (Zhang et al., 2015). In this dataset, the methylation levels of 100 samples are

recorded. For the purpose of comparison, 20% of the CpG sites of $k^* = 50$ samples are held out. We do not hold out more sites in this dataset, because the Methy450K data only contain about 2% Methylation levels in the WGBS whole sequencing dataset.

In Table 2, the prediction based on the nonseparable GaSP model has the lowest RMSE, though the differences with the other methods are smaller compared to the ones in the previous WGBS data since the CpG sites are sparse in this data set, resulting in small site-wise correlations. Modeling both the correlation by site and by sample in the nonseparable GaSP model improves around 10% and 3% in terms of the RMSE compared to the models only exploiting correlation by site and by sample, respectively.

The computation of the nonseparable GaSP model relies heavily on the fast and exact computation algorithm discussed in Section 3. Since the number of methylation levels is at the size of a million in one chromosome in one sample, direct computation of the GaSP model is infeasible. In the supplemental materials, we also compare with a localized Kriging method. The performance of the nonseparable GaSP model is still better, partly because the correlation between CpG sites is long-ranged, shown in the left panel of Figure 1.

6 Concluding remarks

This paper discusses modeling multiple functional data through Gaussian stochastic processes. We unify several different models, including the linear regression model and separable model, through a nonseparable GaSP framework. A computationally efficient algorithm is provided for the large scale problems without approximation to the likelihood. Several interesting future topics are worth exploring from both the computational and modeling perspectives. The achievement in computation is limited, in a sense that the input of the GaSP model (CpG site) is only 1 dimensional. It remains to be an issue to generalize this computational method for the case with multi-dimensional inputs. Some recent progresses

of this direction are introduced in Lindgren et al. (2011), where the GaSP with a Matérn covariance can be represented by stochastic partial differential equations, while a method that computes the exact likelihood is still unknown. Furthermore, the outcomes of methylation levels are $[0, 1]$ with lots of 0 and 1 in the dataset. One may model a point process with probability masses at 0 and 1 to further improve the accuracy in prediction.

Acknowledgements

The research of Mengyang Gu was part of his PhD thesis at Duke University. The authors sincerely thank Barbara Engelhardt for providing the methylation level data and discussion.

References

- Banerjee, S., Gelfand, A. E., Finley, A. O., and Sang, H. (2008). Gaussian predictive process models for large spatial data sets. *Journal of the Royal Statistical Society: Series B (Statistical Methodology)*, 70(4):825–848.
- Bayarri, M. J., Berger, J. O., Calder, E. S., Dalbey, K., Lunagomez, S., Patra, A. K., Pitman, E. B., Spillerh, E. T., and Wolperti, R. L. (2009). Using statistical and computer models to quantify volcanic hazards. *Technometrics*, 51:402–413.
- Conti, S. and O’Hagan, A. (2010). Bayesian emulation of complex multi-output and dynamic computer models. *Journal of statistical planning and inference*, 140(3):640–651.
- Das, P. M. and Singal, R. (2004). DNA methylation and cancer. *Journal of Clinical Oncology*, 22(22):4632–4642.
- Eidsvik, J., Shaby, B. A., Reich, B. J., Wheeler, M., and Niemi, J. (2013). Estimation and

- prediction in spatial models with block composite likelihoods. *Journal of Computational and Graphical Statistics*, 23(2):295–315.
- Gelfand, A. E., Diggle, P., Guttorp, P., and Fuentes, M. (2010). *Handbook of spatial statistics*. CRC Press.
- Gelfand, A. E., Schmidt, A. M., Banerjee, S., and Sirmans, C. (2004). Nonstationary multivariate process modeling through spatially varying coregionalization. *Test*, 13(2):263–312.
- Gu, M. (2016). *Robust uncertainty quantification and scalable computation for computer models with massive output*. PhD thesis, Duke University.
- Gu, M. and Berger, J. O. (2016). Parallel partial Gaussian process emulation for computer models with massive output. *The Annals of Applied Statistics*, 10(3):1317–1347.
- Gu, M., Palomo, J., and Berger, J. O. (2018). Robustgasp: Robust Gaussian stochastic process emulation in r. *arXiv preprint arXiv:1801.01874*.
- Gu, M., Wang, X., and Berger, J. O. (2017+). Robust Gaussian stochastic process emulation. *The Annals of Statistics*.
- Hartikainen, J. and Sarkka, S. (2010). Kalman filtering and smoothing solutions to temporal gaussian process regression models. In *Machine Learning for Signal Processing (MLSP), 2010 IEEE International Workshop on*, pages 379–384. IEEE.
- Higdon, D., Gattiker, J., Williams, B., and Rightley, M. (2008). Computer model calibration using high-dimensional output. *Journal of the American Statistical Association*, 103(482):570–583.
- Kaufman, C. G., Schervish, M. J., and Nychka, D. W. (2008). Covariance tapering for likelihood-based estimation in large spatial data sets. *Journal of the American Statistical Association*, 103(484):1545–1555.

- Liaw, A. and Wiener, M. (2002). Classification and regression by randomforest. *R news*, 2(3):18–22.
- Lindgren, F., Rue, H., and Lindström, J. (2011). An explicit link between gaussian fields and gaussian markov random fields: the stochastic partial differential equation approach. *Journal of the Royal Statistical Society: Series B (Statistical Methodology)*, 73(4):423–498.
- Petris, G., Petrone, S., and Campagnoli, P. (2009). *Dynamic linear models*. Springer.
- Sacks, J., Welch, W. J., Mitchell, T. J., Wynn, H. P., et al. (1989). Design and analysis of computer experiments. *Statistical science*, 4(4):409–423.
- Scarano, M. I., Strazzullo, M., Matarazzo, M. R., and D’Esposito, M. (2005). DNA methylation 40 years later: Its role in human health and disease. *Journal of cellular physiology*, 204(1):21–35.
- West, M. and Harrison, P. J. (1997). *Bayesian Forecasting & Dynamic Models*. Springer Verlag, 2nd edition.
- Whittle, P. (1954). On stationary processes in the plane. *Biometrika*, pages 434–449.
- Whittle, P. (1963). Stochastic process in several dimensions. *Bulletin of the International Statistical Institute*, 40(2):974–994.
- Xu, Y., Xu, Y., and Saria, S. (2016). A bayesian nonparametric approach for estimating individualized treatment-response curves. In *Machine Learning for Healthcare Conference*, pages 282–300.
- Zhang, W., Spector, T. D., Deloukas, P., Bell, J. T., and Engelhardt, B. E. (2015). Predicting genome-wide DNA methylation using methylation marks, genomic position, and DNA regulatory elements. *Genome biology*, 16(14):1–20.

Appendix A: Proofs for Section 2

proof of Lemma 1. Because $\mathbf{A} = \mathbf{U}\mathbf{D}/\sqrt{n}$, $\mathbf{A}(\mathbf{A}^T\mathbf{A})^{-1}\mathbf{A}^T = \mathbf{I}_K$. The likelihood is

$$\begin{aligned}\mathcal{L}(\mathbf{Y}_v(\mathbf{s}^{\mathcal{D}})|\mathbf{v}_v(\mathbf{s}^{\mathcal{D}}), \sigma_0^2) &= (2\pi\sigma_0^2)^{-nK/2} \exp\left(-\frac{(\mathbf{Y}_v(\mathbf{s}^{\mathcal{D}}) - \mathbf{A}_v\mathbf{v}_v(\mathbf{s}^{\mathcal{D}}))^T (\mathbf{Y}_v(\mathbf{s}^{\mathcal{D}}) - \mathbf{A}_v\mathbf{v}_v(\mathbf{s}^{\mathcal{D}}))}{2\sigma_0^2}\right) \\ &= (2\pi\sigma_0^2)^{-nK/2} \exp\left(-\frac{(\hat{\mathbf{v}}_v(\mathbf{s}^{\mathcal{D}}) - \mathbf{v}_v(\mathbf{s}^{\mathcal{D}}))^T \mathbf{A}_v^T \mathbf{A}_v (\hat{\mathbf{v}}_v(\mathbf{s}^{\mathcal{D}}) - \mathbf{v}_v(\mathbf{s}^{\mathcal{D}}))}{2\sigma_0^2}\right),\end{aligned}$$

where $\hat{\mathbf{v}}_v(\mathbf{s}^{\mathcal{D}}) = (\mathbf{A}_v^T \mathbf{A}_v)^{-1} \mathbf{A}_v^T \mathbf{Y}_v(\mathbf{s}^{\mathcal{D}})$. $\mathbf{A}_v^T \mathbf{A}_v$ is a diagonal matrix because

$$\mathbf{A}_v^T \mathbf{A}_v = \begin{pmatrix} (\mathbf{I}_n \otimes \mathbf{a}_1)^T (\mathbf{I}_n \otimes \mathbf{a}_1) & (\mathbf{I}_n \otimes \mathbf{a}_1)^T (\mathbf{I}_n \otimes \mathbf{a}_2) & \dots & (\mathbf{I}_n \otimes \mathbf{a}_1)^T (\mathbf{I}_n \otimes \mathbf{a}_K) \\ (\mathbf{I}_n \otimes \mathbf{a}_2)^T (\mathbf{I}_n \otimes \mathbf{a}_1) & (\mathbf{I}_n \otimes \mathbf{a}_2)^T (\mathbf{I}_n \otimes \mathbf{a}_2) & \dots & (\mathbf{I}_n \otimes \mathbf{a}_2)^T (\mathbf{I}_n \otimes \mathbf{a}_K) \\ \dots & \dots & \dots & \dots \\ (\mathbf{I}_n \otimes \mathbf{a}_K)^T (\mathbf{I}_n \otimes \mathbf{a}_1) & (\mathbf{I}_n \otimes \mathbf{a}_K)^T (\mathbf{I}_n \otimes \mathbf{a}_2) & \dots & (\mathbf{I}_n \otimes \mathbf{a}_K)^T (\mathbf{I}_n \otimes \mathbf{a}_K) \end{pmatrix},$$

with $(\mathbf{I}_n \otimes \mathbf{a}_i)^T (\mathbf{I}_n \otimes \mathbf{a}_i) = (\mathbf{I}_n^T \otimes \mathbf{a}_i^T) (\mathbf{I}_n \otimes \mathbf{a}_i) = (\mathbf{I}_n^T \mathbf{I}_n) \otimes (\mathbf{a}_i^T \mathbf{a}_i)$ and $(\mathbf{I}_n \otimes \mathbf{a}_i)^T (\mathbf{I}_n \otimes \mathbf{a}_j) = (\mathbf{I}_n^T \mathbf{I}_n) \otimes (\mathbf{a}_i^T \mathbf{a}_j) = \mathbf{O}$, where \mathbf{O} is a matrix with each element being 0. Marginalizing out $\mathbf{v}_v(\mathbf{s}^{\mathcal{D}})$, one has

$$\begin{aligned}& \mathcal{L}(\mathbf{Y}_v(\mathbf{s}^{\mathcal{D}})|\sigma_0^2, \sigma_1^2, \dots, \sigma_K^2, \mathbf{R}_1, \dots, \mathbf{R}_K) \\ &= \int \mathcal{L}(\mathbf{Y}_v(\mathbf{s}^{\mathcal{D}})|\mathbf{v}_v(\mathbf{s}^{\mathcal{D}}), \sigma_0^2) p(\mathbf{v}_v(\mathbf{s}^{\mathcal{D}})|\sigma_1^2, \dots, \sigma_K^2, \mathbf{R}_1, \dots, \mathbf{R}_K) d\mathbf{v}_v(\mathbf{s}^{\mathcal{D}}) \\ &= |\mathbf{A}_v^T \mathbf{A}_v|^{-1/2} (2\pi)^{-nK/2} |\boldsymbol{\Sigma}_v + \sigma_0^2 (\mathbf{A}_v^T \mathbf{A}_v)^{-1}|^{-1/2} \exp\left(-\frac{1}{2} \hat{\mathbf{v}}_v(\mathbf{s}^{\mathcal{D}})^T (\boldsymbol{\Sigma}_v + \sigma_0^2 (\mathbf{A}_v^T \mathbf{A}_v)^{-1})^{-1} \hat{\mathbf{v}}_v(\mathbf{s}^{\mathcal{D}})\right) \\ &= |\mathbf{A}_v^T \mathbf{A}_v|^{-1/2} \times \\ & \quad \prod_{i=1}^K \left\{ (2\pi)^{-n/2} |\sigma_i^2 \mathbf{R}_i + \sigma_0^2 (\mathbf{a}_i^T \mathbf{a}_i)^{-1} \mathbf{I}_n|^{-1/2} \exp\left(-\frac{1}{2} \hat{\mathbf{v}}_i(\mathbf{s}^{\mathcal{D}})^T (\sigma_i^2 \mathbf{R}_i + \sigma_0^2 (\mathbf{a}_i^T \mathbf{a}_i)^{-1} \mathbf{I}_n)^{-1} \hat{\mathbf{v}}_i(\mathbf{s}^{\mathcal{D}})\right) \right\}.\end{aligned}$$

The last row follows from the fact that $\hat{\mathbf{v}}_i(\mathbf{s}^{\mathcal{D}})^T$ is the i^{th} row of the matrix $\hat{\mathbf{v}}(\mathbf{s}^{\mathcal{D}})$. \square

proof of Lemma 2. Denote $\mathbf{Y}(\mathbf{s}^{\mathcal{D}}; s_j^*) := [\mathbf{Y}(\mathbf{s}^{\mathcal{D}}); Y(s_j^*)]$ and $\mathbf{v}(\mathbf{s}^{\mathcal{D}}; s_j^*) := [\mathbf{v}(\mathbf{s}^{\mathcal{D}}); v(s_j^*)]$. Both are $k \times (n+1)$ matrices.

Vectorizing the output $\mathbf{Y}_v(\mathbf{s}^{\mathcal{D}}, s_j^*) := \text{vec}(\mathbf{Y}(\mathbf{s}^{\mathcal{D}}, s_j^*))$, a $K \times (n+1)$ vector, and $\mathbf{v}_v(\mathbf{s}^{\mathcal{D}}) := \text{vec}(\mathbf{v}(\mathbf{s}^{\mathcal{D}})^T)$, we can write model (1) as,

$$\mathbf{Y}_v(\mathbf{s}^{\mathcal{D}}, s_j^*) = \mathbf{A}_v \mathbf{v}_v(\mathbf{s}^{\mathcal{D}}, s_j^*) + \boldsymbol{\epsilon},$$

where $\boldsymbol{\epsilon} \sim N(0, \sigma_0^2 \mathbf{I}_{(n+1)K})$. Similar to the proof of Lemma 1, one has

$$L(\mathbf{Y}_v(\mathbf{s}^{\mathcal{D}}, s_j^*) | \boldsymbol{\sigma}_{0:K}^2, \boldsymbol{\gamma}_{1:K}) = |\mathbf{A}_v^T \mathbf{A}_v|^{-1/2} \prod_{i=1}^K p_{MN}(\hat{\mathbf{v}}_i(\mathbf{s}^{\mathcal{D}}, s_j^*); \mathbf{0}, \sigma_i^2 \boldsymbol{\Lambda}_i + \sigma_0^2 (\mathbf{a}_i^T \mathbf{a}_i)^{-1} \mathbf{I}_{n+1}),$$

where $\hat{\mathbf{v}}_i(\mathbf{s}^{\mathcal{D}}, s_j^*)$ is the transpose of the i^{th} row of the $\hat{\mathbf{v}}(\mathbf{s}^{\mathcal{D}}, s_j^*) := (\mathbf{A}^T \mathbf{A})^{-1} \mathbf{A}^T \mathbf{Y}(\mathbf{s}^{\mathcal{D}}, s_j^*)$ and

$$\boldsymbol{\Lambda}_i = \begin{pmatrix} \mathbf{R}_i & \mathbf{r}_i(s_j^*) \\ \mathbf{r}_i^T(s_j^*) & c_i(s_j^*, s_j^*) \end{pmatrix}. \text{ One has}$$

$$\hat{v}_i(s_j^*) | \hat{\mathbf{v}}_i(\mathbf{s}^{\mathcal{D}}), \boldsymbol{\sigma}_0^2, \sigma_i^2, \boldsymbol{\gamma}_i \sim MN(\hat{v}_i^*(s_j^*), \sigma_i^2 c^*(s_j^*) + \sigma_0^2 (\mathbf{a}_i^T \mathbf{a}_i)^{-1}), \quad (20)$$

with $\hat{v}_i^*(s_j^*) = \mathbf{r}_i^T(s_j^*) (\mathbf{R}_i + \frac{\sigma_0^2 (\mathbf{a}_i^T \mathbf{a}_i)^{-1}}{\sigma_i^2} \mathbf{I}_n)^{-1} \hat{\mathbf{v}}_i(\mathbf{s}^{\mathcal{D}})$ and $c_i^*(s_j^*) = c_i(s_j^*, s_j^*) - \mathbf{r}_i^T(s_j^*) (\mathbf{R}_i + \frac{\sigma_0^2 (\mathbf{a}_i^T \mathbf{a}_i)^{-1}}{\sigma_i^2} \mathbf{I}_n)^{-1} \mathbf{r}_i(s_j^*)$.

Note $\mathbf{A}(\mathbf{A}^T \mathbf{A})^{-1} \mathbf{A}^T = \mathbf{I}_K$. One has $\mathbf{Y}(s_j^*) = \mathbf{A} \hat{\mathbf{v}}(s_j^*)$ and $\mathbf{Y}(s^{\mathcal{D}}) = \mathbf{A} \hat{\mathbf{v}}(s^{\mathcal{D}})$. Applying the properties of multivariate normal distribution to (20) leads to the results.

□

Appendix B: Closed form quantities of the continuous state space model

We derive the quantities of continuous state space model representation in (13) in this section.

The following results hold for every subscript i , $1 \leq i \leq k$, so the subscript is dropped for

simplicity. The SDE is

$$\frac{d\boldsymbol{\theta}(s)}{ds} = \mathbf{J}\boldsymbol{\theta}(s) + \mathbf{L}z(s),$$

where

$$\mathbf{J} = \begin{pmatrix} 0 & 1 & 0 \\ 0 & 0 & 1 \\ -\lambda^3 & -\lambda^2 & -3\lambda \end{pmatrix},$$

and $\mathbf{L} = (0, 0, 1)^T$.

Denote $d_j = |s_j - s_{j-1}|$. We have

$$e^{\mathbf{J}d_j} = \frac{e^{-\lambda d_j}}{2} \begin{pmatrix} \lambda^2 d_j^2 + 2\lambda + 2 & 2(\lambda d_j^2 + d_j) & d_j^2 \\ -\lambda^3 d_j^2 & -2(\lambda^2 d_j^2 - \lambda d_j - 1) & 2d_j - \lambda d_j^2 \\ \lambda^4 d_j^2 - 2\lambda^3 d_j & 2(\lambda^3 d_j^2 - 3\lambda^2 d_j) & \lambda^2 d_j^2 - 4\lambda d_j + 2 \end{pmatrix}$$

$$\mathbf{Q}(s_j) = \frac{4\sigma^2 \lambda^5}{3} \begin{pmatrix} Q_{1,1}(s_j) & Q_{1,2}(s_j) & Q_{1,3}(s_j) \\ Q_{2,1}(s_j) & Q_{2,2}(s_j) & Q_{2,3}(s_j) \\ Q_{3,1}(s_j) & Q_{3,2}(s_j) & Q_{3,3}(s_j) \end{pmatrix},$$

with

$$\begin{aligned}
Q_{1,1}(s_j) &= \frac{e^{-2\lambda d_j}(3 + 6\lambda d_j + 6\lambda^2 d_j^2 + 4\lambda^3 d_j^3 + 2\lambda^4 d_j^4) - 3}{-4\lambda^5}, \\
Q_{1,2}(s_j) = Q_{2,1}(s_j) &= \frac{e^{-2\lambda d_j} d_j^4}{2}, \\
Q_{1,3}(s_j) = Q_{3,1}(s_j) &= \frac{e^{-2\lambda d_j}(1 + 2\lambda d_j + 2\lambda^2 d_j^2 + 4\lambda^3 d_j^3 - 2\lambda^4 d_j^4) - 1}{4\lambda^3}, \\
Q_{2,2}(s_j) &= \frac{e^{-2\lambda d_j}(1 + 2\lambda d_j + 2\lambda^2 d_j^2 - 4\lambda^3 d_j^3 + 2\lambda^4 d_j^4) - 1}{-4\lambda^3}, \\
Q_{2,3}(s_j) = Q_{3,2}(s_j) &= \frac{e^{-2\lambda d_j} d_j^2(4 - 4\lambda d_j + \lambda^2 d_j^2)}{2}, \\
Q_{3,3}(s_j) &= \frac{e^{-2\lambda d_j}(-3 + 10\lambda^2 d_j^2 - 22\lambda^2 d_j^2 + 12\lambda^2 d_j^2 - 2\lambda^4 d_j^4) + 3}{4\lambda},
\end{aligned}$$

and

$$\mathbf{Q}(s_0) = \begin{pmatrix} \sigma^2 & 1 & -\sigma^2 \lambda^2 / 3 \\ 0 & \sigma^2 \lambda^2 / 3 & 1 \\ -\sigma^2 \lambda^2 / 3 & 0 & \sigma^2 \lambda^4 \end{pmatrix}.$$

The joint distribution of $\boldsymbol{\theta}(s_{0:n})$ is given by

$$\begin{pmatrix} \boldsymbol{\theta}(s_0) \\ \boldsymbol{\theta}(s_1) \\ \boldsymbol{\theta}(s_2) \\ \dots \\ \boldsymbol{\theta}(s_n) \end{pmatrix} \sim MN \left(\begin{pmatrix} 0 \\ 0 \\ 0 \\ \dots \\ 0 \end{pmatrix}, \begin{pmatrix} \mathbf{Q}(s_0)^{-1} & -\mathbf{G}^T(s_1)\mathbf{Q}(s_1)^{-1}\mathbf{G}(s_1) & & & \\ -\mathbf{G}^T(s_1)\mathbf{Q}(s_1)^{-1}\mathbf{G}(s_1) & \mathbf{Q}^{-1}(s_1) & -\mathbf{G}^T(s_2)\mathbf{Q}(s_2)^{-1}\mathbf{G}(s_2) & & \\ & -\mathbf{G}^T(s_2)\mathbf{Q}(s_2)^{-1}\mathbf{G}(s_2) & \mathbf{Q}^{-1}(s_2) & \dots & \\ & & \dots & \dots & \dots \\ & & & & \mathbf{Q}^{-1}(s_n) \end{pmatrix}^{-1} \right).$$